Japanese Journal of Applied Physics

RAPID COMMUNICATIONS

Multi-band coherent perfect absorption excited by a multi-sized and multilayer metasurface

To cite this article: Sha Huang *et al* 2018 *Jpn. J. Appl. Phys.* **57** 090304

Japanese Journal of Applied Physics **57**, 090304 (2018)
https://doi.org/10.7567/JJAP.57.090304

RAPID COMMUNICATION

Multi-band coherent perfect absorption excited by a multi-sized and multilayer metasurface

Sha Huang, Ling Li*, Weidong Chen, Jinqiao Lei, Fengling Wang, Ke Liu, and Zhengwei Xie*

College of Physics and Electronic Engineering, Sichuan Normal University, Chengdu 610101, China

*E-mail: lingli70@aliyun.com; zzwxie@aliyun.com

Received May 3, 2018; accepted July 10, 2018; published online July 27, 2018

We propose a multi-band infrared coherent perfect absorber where four perfect absorption peaks can be obtained for antisymmetrical inputs. The FWHM is nearly four times larger than that of a single band absorber. In addition, the absorptivity of each peak can be independently tuned by phase modulation. Since only magnetic resonances in the form of catenary optical fields in the upper and lower dielectric layers can be excited for symmetrical inputs, the number of absorption peaks will be reduced by half at this time. The absorption frequency under symmetrical inputs can be flexibly selected from low frequency to high frequency by changing the material of the upper and lower dielectric layers. Moreover, the bandwidth in optimized broadband absorber is enhanced by 9 times while high absorbance is maintained. The characteristic of the enhancing absorption bandwidth and the selective absorption may allow our metasurface to be used in many applications such as optical switch and modulators.

The field of planar metamaterials[1,2] or metasurfaces[3–6] has been widely studied in recent years owing to their unusual functionality which are not found in natural materials, such as negative refractive index,[7,8] invisibility cloaking,[9] and focusing of electromagnetic waves.[10] Since metamaterials or metasurfaces can modulate the amplitude, phase and polarization of electromagnetic waves in a desired way, many relevant applications can be achieved including perfect absorbers,[11] electromagnetic stealth,[12] nonlinear optics,[13] and thermal emitters.[14]

As a practical application, perfect absorption of light is of great importance in plasmonic sensor[15] and electromagnetic stealth.[16] Thus metamaterial perfect absorbers[11,17–20] which can control the amplitude of electromagnetic waves have attracted more and more attention and been widely studied from microwave to visible frequencies. However, the absorptivity of these metamaterial absorbers is very fixed which is dependent on the original structure, thus it is not suitable for some applications that require flexible tunability for absorption.

The recently proposed coherent perfect absorption (CPA)[21–27] can dynamically control the absorptivity by changing the relative phase of two coherent counter-propagating incident beams. This additional tunability for absorption is useful in many applications including optical switches or modulators.[28] One drawback of the initial CPA is that its absorption bandwidth is very narrow. Although many researches have been done on broadband CPA including doped silicon film[22] and multilayer doped indium tin oxide (ITO),[29] the bandwidth or spectral selectivity still cannot meet the requirement of broadband absorption applications.

In this paper, we propose a new absorber in which the CPA bandwidth can be significantly broadened in infrared under anti-symmetrical inputs. The absorber is composed of laterally multi-sized subunits and vertically stacked multilayer structures in a unit cell. The numerical results show that the coherent absorption is dependent on both the material of the dielectric layer and the size of the subunits. In addition, the number of absorption peaks will reduce by half when the phase difference changes from 180 to 0° and the frequency of the remaining absorption peak under symmetrical inputs can be flexibly selected, which is determined by the material of the upper and lower dielectric layers. Thus selective absorption is achieved which is of great importance to explore spectroscopic applications. Due to the fact that both the size and material have independent effects on absorption frequency, the coherent controllable multi-band perfect absorber we propose here can provide a useful reference for the design of broadband coherent perfect absorber at other desired frequencies.

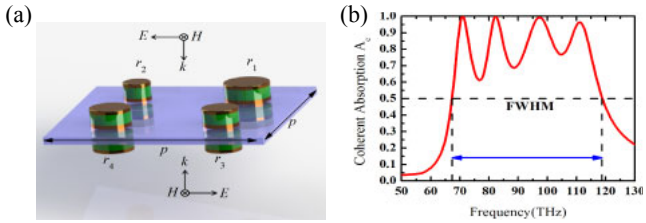

Fig. 1. (Color online) (a) Schematics of the unit cell in multi-sized and multilayer absorber and the propagation configurations. (b) Coherent absorption spectra of the multi-sized and multilayer absorber at normal incidence.

As shown in Fig. 1(a), the proposed metasurface is composed of laterally multi-sized subunits and vertically stacked multilayer structures in a unit cell, which is illuminated by two anti-symmetric coherent incident beams whose phase difference is 180°. The upper and lower circular patches pairs are periodically patterned on both sides of the middle dielectric layer within a period $p = 2.4\,\mu$m. The radius of circular patches in four subunits are r_1, r_2, r_3, r_4, respectively. The upper and lower dielectric layers are chosen as ZnTe whose refractive index is 2.6 within the considered frequency range. And Al_2O_3 is used to the middle dielectric layer whose dielectric constants and loss tangent are 2.28 and 0.04. All metal parts are gold with thickness $t = 0.04\,\mu$m and experimental value of permittivity is used.[30] For simplicity, we first simulate the metasurface in which the radius $r_1 = r_4 = 0.42\,\mu$m and $r_2 = r_3 = 0.36\,\mu$m. To satisfy the condition of CPA, the thickness of ZnTe layers (d) and Al_2O_3 layer (h) are optimized to 150 and 95 nm, respectively. Based on full-wave simulations using CST Microwave Studio, the absorption spectra of the metasurface at normal incidence is shown in Fig. 1(b). Four distinct absorption peaks at the frequencies of 71, 82.2, 97.4, and 111.2 THz with absorptivity of 99.98, 99.87, 99.31, and 96.38% can be observed. The full width half maximum (FWHM) in such a two-sized multilayer metasurface is extended to 51.4 THz, which is obviously increased and nearly four times larger than that of a single

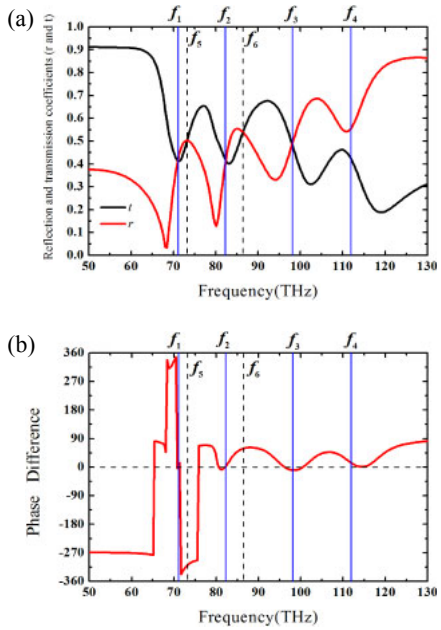

Fig. 2. (Color online) (a) Amplitudes of reflection (Red line) and transmission coefficients (Blue line) for a single beam incident normally upon the metasurface. (b) The corresponding phase difference of reflection and transmission coefficients. The blue line indicate the position of the four absorption peaks with the frequencies of 71, 82.2, 97.4, and 111.2 THz, respectively.

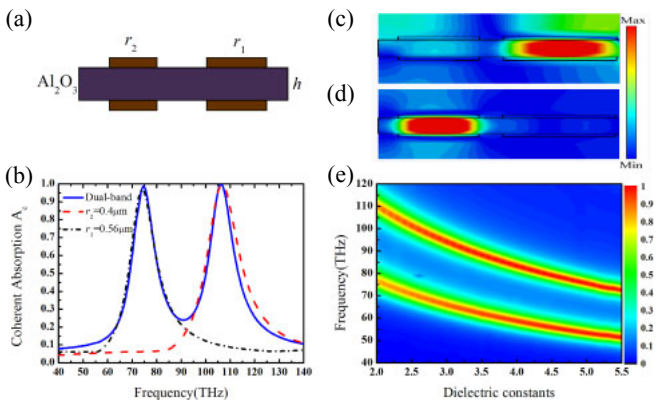

Fig. 3. (Color online) (a) Side schematic of the multi-sized dual-band absorber. (b) Coherent absorption spectra of the multi-sized dual-band absorber at normal incidence. Distributions of the magnetic field at two resonant frequencies of (c) 74.6 THz and (d) 106.2 THz. (e) Absorption spectra of the multi-sized dual-band absorber with varying the dielectric constants of the dielectric layer while keeping the other parameter fixed.

band absorber. Actually, the metasurface we designed here is better than the previous multi-band coherent perfect absorber in Ref. 23 whose FWHM is only 26.7 THz.

As mentioned in previous work, coherent perfect absorption needs to meet two conditions: (a) forward and backward waves are of the same amplitudes and (b) reflection and transmission coefficients have same amplitudes ($r = t$) and $n\pi$ phase difference with n being an arbitrary integer when illuminated by a single beam.[26] During the simulation, the two incident beams in opposite directions are set to the same intensity, thus the first condition is satisfied. Figures 2(a) and 2(b) show the reflection and transmission coefficients of the metasurface for a single beam incident and the corresponding phase difference. It is clear that the reflection coefficient is equal to the transmission coefficient and the corresponding phase differences are close to 0 at the frequencies of f_1, f_2, and f_3. Therefore, the two conditions of coherent perfect absorption are both satisfied, there are three absorption peaks with absorptivity greater than 99%. Unfortunately, at the frequency of f_4 although the phase difference is close to 0, the reflection coefficient has a difference with transmission coefficient and the absorptivity will decrease which is only 96.38%. However, considering the influence of the above two conditions, the absorptivity at the frequency of f_4 is still the largest in the frequency range around it, and thus exhibits an absorption peak in the spectrum. In addition, it is worth mentioning that although the reflection and transmission coefficient is equal at frequencies f_5 and f_6, the corresponding phase difference is far away from $n\pi$ and therefore there is no perfect absorption at these two frequencies.

To explain the physical mechanism of the above multi-band coherent perfect absorption, we first investigate the multi-sized dual-band absorber, as shown in Fig. 3(a). The dielectric layer is chosen as Al_2O_3 with thickness $h = 200$ nm and the radius of each patches pair are $r_1 = 0.56$ µm and $r_2 = 0.4$ µm, respectively. Figure 3(b) shows the absorption spectra of the multi-sized dual-band absorber at normal incidence. Two distinct absorption peaks located at 74.6 and 106.2 THz with absorptivity of 98.61 and 99.88% can be observed.

To illustrate the reason for the appearance of two peaks, we simulated the metasurface with only one subunit whose radius is r_1 or r_2. As shown in Fig. 3(b), the red dashed line and black dotted line represent the absorption spectra of only small or large radius in one subunit, respectively. It is clear that only one peak can be observed in such a metasurface. The comparison of these simulation results shows that the appearance of the two absorption peaks in dual-band absorber is a result of the superposition of the peaks caused by two subunits of different radius.

In order to better illustrate the nature of dual-band absorption, the magnetic field distributions at two absorption peaks are shown in Figs. 3(c) and 3(d), which resemble the catenary optical fields in plasmonic structures.[31] For the anti-symmetric two incident beams, the electric field vector vibrates in the opposite direction, thus the opposite flowing surface current are formed in the upper and lower metal patches. The reverse current forms a current loop and then produces a magnetic dipole in the dielectric layer, which can couple with the incident magnetic field to generate a magnetic resonance. The resonance will result in a distinct enhancement of absorption. In Fig. 3(c), it is clear that the magnetic field is strongly confined under the larger metal circular patch and within the dielectric layer at resonance frequency of 74.6 THz. The similar behavior can be found at the resonance frequency of 106.2 THz in Fig. 3(d), except that resonance occurs under the smaller metal circular patch. Since the resonances cannot affect each other, the magnetic field distribution again confirms the superposition relationship for the appearance of dual-band absorption.

To provide a material selectivity in the experiment, the effect of dielectric material on absorption is investigated. It is found that a linear relationship is existed between resonant frequency and dielectric constant of material. Figure 3(e) shows the absorption spectra of multi-sized metasurface as the dielectric constant changes from 2 to 5.5, while geometric parameters remain unchanged. Both absorption peaks move toward low frequency as the dielectric constant increases,

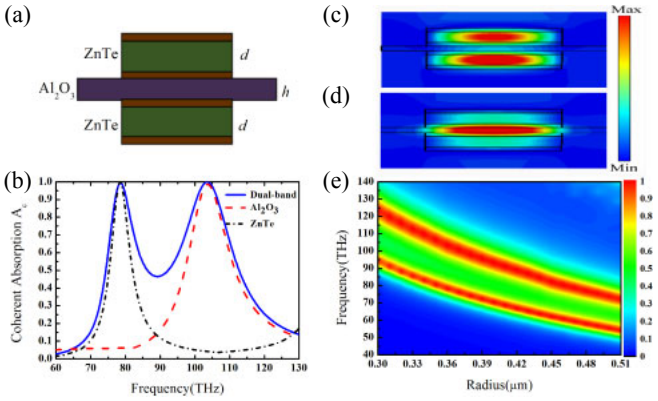

Fig. 4. (Color online) (a) Side schematics of the multilayer dual-band absorber. (b) Coherent absorption spectra of the multilayer dual-band absorber at normal incidence. Distributions of the magnetic field at two resonant frequencies of (c) 78.6 THz and (d) 103.6 THz. (e) Absorption spectra of the multilayer dual-band absorber with various the radius of circular patch while keeping the other parameter unchanged.

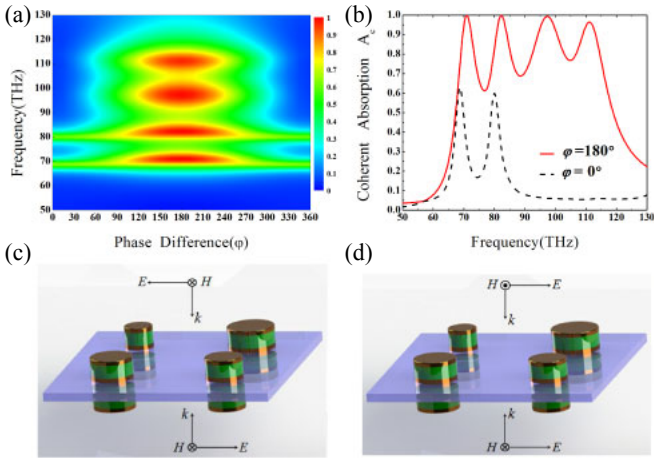

Fig. 5. (Color online) (a) Coherent absorptivity of the multi-sized and multilayer absorber as a function of frequency and phase difference. (b) Absorption spectra for anti-symmetrical (phase difference is 180°) and symmetrical (phase difference is 0°) inputs. (c) The propagation configurations of anti-symmetrical inputs (defined according to the symmetry of electric fields). The incident electric field is reversed while the incident magnetic field is in the same direction. (d) The propagation configurations of symmetrical inputs. The incident electric field is in the same direction while the incident magnetic field is reversed.

which can provide a useful reference for further achieving multi-band coherent perfect absorption.

In order to obtain the better frequency adjustability of absorber, based on the above results, the dual-band absorber consisting of vertical stacked multilayer structure is proposed further and shown in Fig. 4(a). Similarly, two anti-symmetric coherent beams are used as excitations. The radius of circular patch is set to 0.36 μm and other geometry parameters such as p and t are unvaried. Actually, the material have not been changed compared with multi-sized and multilayer metasurface. To meet the CPA conditions, the thicknesses of ZnTe and Al_2O_3 layers are adjusted to $d = 115$ nm and $h = 55$ nm. Fig. 4(b) shows the absorption spectra of the multilayer dual-band absorber at normal incidence. Two distinct absorption peaks located at 78.6 and 103.6 THz can be observed with absorptivity of 99.43 and 99.95%, respectively. Furthermore, to explain the reason for the appearance of double peaks, the absorption spectra of the metasurface with only a single metal–dielectric–metal pair for different dielectric materials is simulated. In the inset of Fig. 4(b), the black dotted line and red dashed line indicate the absorption spectra of one metal–dielectric–metal pair with the materials of ZnTe and Al_2O_3, respectively. Similar to multi-sized absorber, the appearance of dual-band absorption in multilayer metasurface is also by reason of the superposition of these two separate absorption peaks.

In addition, to get insight into the physical mechanism of dual-band absorption in multilayer metasurface, Figs. 4(c) and 4(d) show the magnetic field distributions at two resonant frequencies of 78.6 and 103.6 THz. The magnetic field is strongly concentrated in the ZnTe dielectric layers at low frequency while in the Al_2O_3 layer at high frequency, respectively. It indicates that dielectric layers of different materials can bind light of different frequencies in multilayer metasurface.

Similarly, the influence of circular patch radius on absorption is investigated in multilayer dual-band absorber. Figure 4(e) shows the absorption spectrum as a function of radius and frequency. As the radius increases, both magnetic resonance will shift to low frequencies at the same time. This relationship can also be seen in multi-size metasurface. The ability of dielectric material and circular patch radius to tune the resonant frequency can be effectively utilized to broaden the bandwidth of coherent perfect absorption. Combined with the above analysis, the appearance of four absorption peaks in multi-sized and multilayer absorber is thanks to the dual influence of two dielectric materials and two-sized subunits.

Moreover, as mentioned above, a significant advantage of CPA is that its absorptivity can be flexibly tuned, which may be useful in absorption modulators or optical switches. The modulation ability of the multi-sized and multilayer metasurface is investigated in Fig. 5(a). When the phase difference changes, the absorptivity of four absorption peaks will be tuned simultaneously. To better illustrate the effect of phase difference on absorption, the absorption spectra at two specific conditions with anti-symmetrical ($\varphi = 180°$) and symmetrical ($\varphi = 0°$) inputs is separately shown in Fig. 5(b). The symmetric and anti-symmetric inputs are defined in terms of the electric-field vectors. Figures 5(c) and 5(d) illustrate the corresponding propagation configurations, respectively. For symmetric inputs, the direction of E vector is the same while the direction of H vector is opposite. For anti-symmetric inputs, the direction of E vector is opposite while the direction of H vector is the same. Figure 5(b) shows that two absorption peaks disappear while two weaker absorption peaks appear for symmetrical inputs.

To elucidate the physical mechanism for this change, the absorption spectra in multilayer structure under symmetrical and antisymmetrical conditions is investigated. As shown in Fig. 6(a), the influence of phase difference on absorption is similar to that in multi-sized and multilayer absorber. The magnetic field distributions in Fig. 6(b) show that magnetic resonance in ZnTe and Al_2O_3 layers both can be excited when the phase difference is 180°. Since the material has a linear relationship with the resonant frequency as described above, the magnetic field are strongly confined in the upper and lower ZnTe dielectric layers at low frequency while bound to the intermediate Al_2O_3 layer at high frequency. However, when the phase difference is 0°, the resonance occurs only in the upper and lower dielectric layers. Therefore there is only

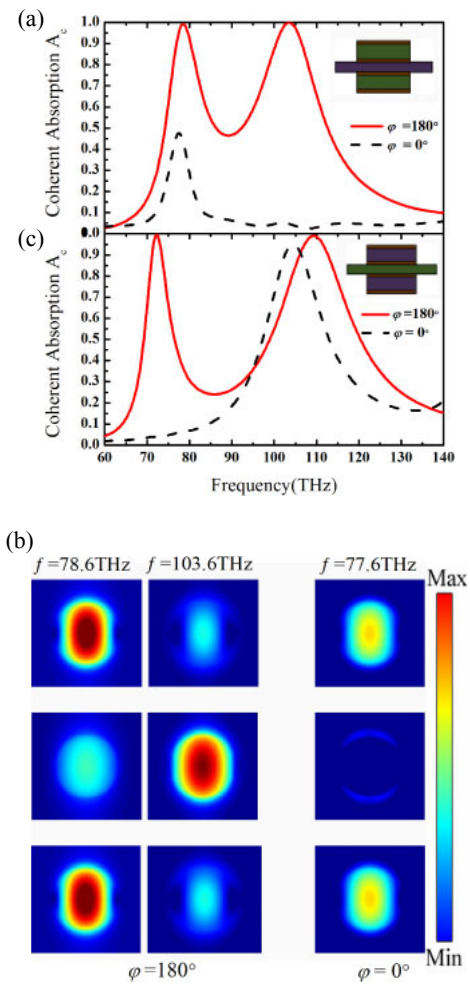

Fig. 6. (Color online) (a) Coherent absorption spectra of the multilayer absorber at normal incidence under anti-symmetrical and symmetrical conditions. Inset is ZnTe–Al_2O_3–ZnTe multilayer structure. (b) Distributions of the magnetic field in the upper ZnTe, middle Al_2O_3, and lower ZnTe dielectric layers at the frequencies of 78.6 and 103.6 THz when the phase difference is 180°, and 77.6 THz when the phase difference is 0°. (c) Coherent absorption spectra of the multilayer absorber at normal incidence. Inset is Al_2O_3–ZnTe–Al_2O_3 multilayer structure.

one absorption peak corresponding to the material of ZnTe at low frequency in this multilayer structure. The reason why the absorptivity of this peak is relatively small is that the magnetic resonance in ZnTe layers is weak in this case.

In order to illustrate that the frequency of absorption peak under symmetrical inputs is related to the material of the upper and lower dielectric layers, another multilayer metasurface in which the ZnTe and Al_2O_3 materials are exchanged is simulated. Figure 6(c) shows the absorption spectra. Another absorption peak corresponding to the material of Al_2O_3 can be observed at high frequency. This change again confirms that resonance occurs only in the upper and lower dielectric layers for symmetrical inputs, and the position of absorption peak is affected by the placement of dielectric material.

The above studies show that in multilayer structure, the beams of two specific frequencies both can be absorbed for anti-symmetrical inputs. However, beams of one frequency are absorbed and beams of another frequency pass completely for symmetrical inputs. The frequency of absorbed beams under symmetrical conditions can be flexibly controlled by changing the dielectric material. For example, if high-frequency beams

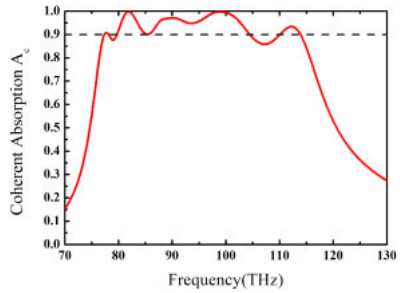

Fig. 7. (Color online) Absorption spectra of the broadband absorber at normal incidence.

are desired to be absorbed, we can simply select a material with a lower dielectric constant for the upper and lower dielectric layers. In view of these two characteristics, selective absorption can be achieved in our design metasurface.

Based on the analysis of the above results, the changes of the dielectric material in multi-size dual-band absorber and the patches radius in multilayer dual-band absorber both can lead to the movement of absorption peak. We adjust the radius r_1, r_2, r_3, r_4 in multi-sized and multilayer metasurface to 0.4, 0.34, 0.35, and 0.38 µm, respectively and use the optimized thickness $d = 205$ nm and $h = 95$ nm to achieve broadband absorption. The simulated broadband absorption spectrum is shown in Fig. 7. The bandwidth as the frequency range with absorptivity greater than 90% is 28.2 THz in our proposed broadband absorber, which is nine times larger than that of a single band absorber and expanded to more than three times compared with the former absorber in Ref. 23 whose bandwidth merely possess 9 THz. This remarkable ability to broaden the absorption bandwidth allows our designed absorber to be applied to many broadband applications.

In summary, we have designed a multi-sized and multilayer metasurface and numerically demonstrated that multi-band coherent perfect absorption under anti-symmetrical inputs can be achieved in the infrared. Compared with traditional absorbers, the FWHM in our designed structure is significantly enhanced. Importantly, the absorptivity can be dynamically tuned in this multi-band absorber by changing the phase difference between two input beams. In particular, due to the excited magnetic resonance at different dielectric layers, half of the absorption peaks will disappear under symmetrical inputs. The frequency of the remaining absorption peak can be flexibly selected by changing the material of the upper and lower dielectric layers. Thus selective coherent perfect absorption is realized, which may be promising candidates for optical switches or modulator. Moreover, It is further shown that broadband absorption can be achieved when the radius of circular patches are optimized, the absorption bandwidth is enhanced by nine times compared with that in single-band absorption, which may be useful in broadband applications. Combined with the dual impact of material and structural dimensions, our proposed scheme can provide a reference to broaden the absorption bandwidth at other desired frequencies and for practical engineering application.[32)]

Acknowledgments This work was supported by 973 Program of China (Grant No. 2013CBA01700); Sichuan Provincial Department of Education (Grant No. 16ZA0047); the Large Precision Instruments Open Project Foundation of Sichuan Normal University (Grant Nos. DJGX2017050, DJGX2017051, DJGX2017052); Postgraduate Excellent Paper Nurturing Fund of Sichuan Normal University; Sichuan Science and Technology Program (Grant No. 2018JY0439).

1) N. Engheta and R. W. Ziolkowski, *Metamaterials: Physics and Engineering Explorations* (Wiley-IEEE Press, New York, 2006).
2) R. A. Shelby, D. R. Smith, and S. Schultz, Science **292**, 77 (2001).
3) N. Yu and F. Capasso, Nat. Mater. **13**, 139 (2014).
4) Y. Yang, W. Wang, A. Boulesbaa, I. I. Kravchenko, D. P. Briggs, A. Puretzky, D. Geohegan, and J. Valentine, Nano Lett. **15**, 7388 (2015).
5) M. Pu, X. Li, X. Ma, Y. Wang, Z. Zhao, C. Wang, C. Hu, P. Gao, C. Huang, H. Ren, X. Li, F. Qin, J. Yang, M. Gu, M. Hong, and X. Luo, Sci. Adv. **1**, e1500396 (2015).
6) X. Luo, Sci. China Phys. Mech. Astron. **58**, 594201 (2015).
7) S. Zhang, Y. S. Park, J. Li, X. Lu, W. Zhang, and X. Zhang, Phys. Rev. Lett. **102**, 023901 (2009).
8) E. Plum, J. Zhou, J. Dong, V. A. Fedotov, T. Koschny, C. M. Soukoulis, and N. I. Zheludev, Phys. Rev. B **79**, 035407 (2009).
9) Y. M. Liu and X. Zhang, Chem. Soc. Rev. **40**, 2494 (2011).
10) X. Li, S. Xiao, B. Cai, Q. He, T. Cui, and L. Zhou, Opt. Lett. **37**, 4940 (2012).
11) N. I. Landy, S. Sajuyigbe, J. J. Mock, D. R. Smith, and W. J. Padilla, Phys. Rev. Lett. **100**, 207402 (2008).
12) C. Pfeiffer and A. Grbic, Phys. Rev. Lett. **110**, 197401 (2013).
13) M. W. Klein, C. Enkrich, M. Wegener, and S. Linden, Science **313**, 502 (2006).
14) M. Diem, T. Koschny, and C. M. Soukoulis, Phys. Rev. B **79**, 033101 (2009).
15) N. Liu, M. Mesch, T. Weiss, M. Hentschel, and H. Giessen, Nano Lett. **10**, 2342 (2010).
16) S. Li, J. Luo, S. Anwar, S. Li, W. Lu, Z. H. Hang, Y. Lai, B. Hou, M. Shen, and C. Wang, Sci. Rep. **4**, 7369 (2014).
17) C. M. Watts, X. Liu, and W. J. Padilla, Adv. Mater. **24**, OP98 (2012).
18) Y. Huang, M. Pu, P. Gao, Z. Zhao, X. Li, X. Ma, and X. Luo, Appl. Phys. Express **10**, 112601 (2017).
19) K. Halterman and J. M. Elson, Opt. Express **22**, 7337 (2014).
20) M. Pu, C. Hu, M. Wang, C. Huang, Z. Zhao, C. Wang, Q. Feng, and X. Luo, Opt. Express **19**, 17413 (2011).
21) Y. D. Chong, L. Ge, H. Cao, and A. D. Stone, Phys. Rev. Lett. **105**, 053901 (2010).
22) M. Pu, Q. Feng, M. Wang, C. Hu, C. Huang, X. Ma, Z. Zhao, C. Wang, and X. Luo, Opt. Express **20**, 2246 (2012).
23) S. Huang, Z. Xie, W. Chen, J. Lei, F. Wang, K. Liu, and L. Li, Opt. Express **26**, 7066 (2018).
24) W. Wan, Y. Chong, L. Ge, H. Noh, A. D. Stone, and H. Cao, Science **331**, 889 (2011).
25) C. Yan, M. Pu, J. Luo, Y. Huang, X. Li, X. Ma, and X. Luo, Opt. Laser Technol. **101**, 499 (2018).
26) W. Zhu, F. Xiao, M. Kang, and M. Premaratne, Appl. Phys. Lett. **108**, 121901 (2016).
27) G. Nie, Q. Shi, Z. Zhu, and J. Shi, Appl. Phys. Lett. **105**, 201909 (2014).
28) X. Fang, M. L. Tseng, J. Ou, K. F. MacDonald, D. P. Tsai, and N. I. Zheludev, Appl. Phys. Lett. **104**, 141102 (2014).
29) T. Y. Kim, M. A. Badsha, J. Yoon, S. Y. Lee, Y. Jun, and C. K. Hwangbo, Sci. Rep. **6**, 22941 (2016).
30) D. Edwards, in *Handbook of Optical Constants of Solids*, ed. E. Palik (Academic Press, New York, 1985) p. 286.
31) M. Pu, Y. Guo, X. Li, X. Ma, and X. Luo, ACS Photonics **10**, 1021 (2018).
32) X. Luo, Adv. Opt. Mater. **6**, 1701201 (2018).